

## MIT Open Access Articles

*Coupled-Magnetic Filters With Adaptive Inductance Cancellation*

The MIT Faculty has made this article openly available. **Please share** how this access benefits you. Your story matters.

**Citation:** Lymar, Daria S., Timothy C. Neugebauer, and David J. Perreault. "Coupled-Magnetic Filters With Adaptive Inductance Cancellation." IEEE Trans. Power Electron. 21, no. 6 (n.d.): 1529–1540. © 2006 IEEE

**As Published:** <http://dx.doi.org/10.1109/TPEL.2006.882975>

**Publisher:** Institute of Electrical and Electronics Engineers (IEEE)

**Persistent URL:** <http://hdl.handle.net/1721.1/86966>

**Version:** Final published version: final published article, as it appeared in a journal, conference proceedings, or other formally published context

**Terms of Use:** Article is made available in accordance with the publisher's policy and may be subject to US copyright law. Please refer to the publisher's site for terms of use.



# Coupled-Magnetic Filters With Adaptive Inductance Cancellation

Daria S. Lyman, Timothy C. Neugebauer, *Member, IEEE*, and David J. Perreault, *Senior Member, IEEE*

**Abstract**—Conventional filter circuits suffer from a number of limitations, including performance degradation due to capacitor parasitic inductance and the size and cost of magnetic elements. Coupled-magnetic filters have been developed that provide increased filter order with a single magnetic component, but also suffer from parasitic inductance in the filter shunt path due to imperfectly-controlled coupling of the magnetics. In this paper, we introduce a new approach to coupled-magnetic filters that overcomes these limitations. Filter sensitivity to variations in coupling is overcome by adaptively tuning the magnetic circuit for minimum rms ripple performance with feedback based on the sensed filter output ripple. This active control enables much greater robustness to manufacturing and environmental variations than is possible in the conventional “zero-ripple” coupled-magnetic approach, while preserving its advantages. Moreover, the proposed technique also adaptively cancels the deleterious effects of capacitor parasitic inductance, thereby providing much higher filter performance than is achievable in conventional designs. The new technique is experimentally demonstrated in a dc–dc power converter application and is shown to provide high performance.

**Index Terms**—Automatic tuning, coupled inductor filter, integrated magnetics, zero-ripple filter.

## I. INTRODUCTION

**E**LECTRICAL filters are an integral part of most electronic systems, and are particularly important in power electronics. Control of switching ripple is the primary factor in sizing the magnetics and filter components that comprise much of the size, mass, and cost of a power converter. Design techniques that mitigate converter ripple are therefore valuable for reducing the size of power electronics and the amount of electromagnetic interference (EMI) that is generated.

The low-pass filters used in power electronics typically employ capacitors as shunt elements and magnetics, such as inductors, as series-path elements. The attenuation of a filter stage is determined by the amount of impedance mismatch between the series and shunt paths. Minimizing shunt-path impedance and maximizing series-path impedance at high frequencies are thus important design goals. An important limitation of conventional filters is the effect of filter capacitor parasitic inductance, which increases shunt path impedance at high frequencies

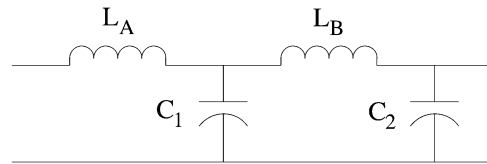


Fig. 1. Example of a multisection filter.

[1]–[5]. Common methods for overcoming the deteriorated filter performance caused by capacitor parasitic inductance include placing various types of capacitors in parallel to cover different frequency ranges, and increasing the order of the filter network. Both approaches increase filter size and cost.

The size of magnetic components is also of importance, particularly in multisection filters, such as that illustrated in Fig. 1. One technique that has been explored for reducing magnetic component count and size is the use of coupled magnetics (e.g., by realizing inductors  $L_A$  and  $L_B$  in Fig. 1 with a coupled magnetic circuit wound on a single core). Coupled magnetics have been used with capacitors to achieve “notch” filtering [6]–[9], as well as so-called “zero-ripple” filtering [10]–[14]. Despite the name “zero-ripple,” it has been shown that the performance of these coupled-magnetic filters is equivalent to filters without magnetically-coupled windings [10], [11]. The advantage of coupled-magnetic filters is that they enable a high-order filter structure to be realized with a single magnetic component. However, they suffer from the fact that their performance depends on very precise coupling within the magnetic circuit. Any mismatch in this coupling, such as that induced by small material or manufacturing variations, temperature changes, or variations in operating point, can dramatically reduce ripple attenuation. The sensitivity of this approach to magnetic coupling has limited its value in many applications, despite its other advantages.

In this paper, we introduce a new approach to coupled-magnetic filters that overcomes the limitations described above. Filter sensitivity to variations in coupling is overcome by adaptively tuning the net shunt-path inductance with feedback based on the sensed filter output ripple. Unlike previous active tuning methods [8], [9], [15], the approach implemented here both tunes for “zero-ripple” performance and automatically compensates for filter parasitic inductance. This active control enables much greater robustness to manufacturing and environmental variations than is possible in the conventional coupled-magnetic approach, while preserving its advantages. Moreover, as will be shown, the proposed technique also adaptively cancels the deleterious effects of capacitor parasitic inductance. Equivalent series inductance is a dominant performance limitation of

Manuscript received May 17, 2005; revised January 4, 2006. This paper was presented in part at the IEEE Power Electronic Specialists Conference, Recife, Brazil, June 2005. This work was supported by the United States Office of Naval Research under ONR Grant N00014-02-1-0481. Recommended by Associate Editor C. R. Sullivan.

D. S. Lyman and D. J. Perreault are with the Beth Israel Deaconness Medical Center, Boston, MA 02215 USA (e-mail: dlyman@mit.edu; djperrea@mit.edu).

T. C. Neugebauer is with the Draper Laboratory, Cambridge, MA 02139 USA.

Digital Object Identifier 10.1109/TPEL.2006.882975

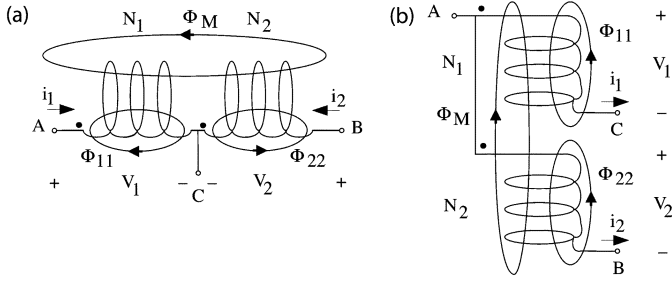


Fig. 2. (a) Coupled magnetic windings in a center-tapped connection. (b) Coupled magnetic windings in an end-tapped connection.

large-valued film and ceramic capacitors at high frequencies (e.g., [16], [17]), and it can also be a significant limitation (over capacitor ESR) in electrolytic capacitors at sufficiently high frequencies. Thus, the proposed approach can provide much higher filter performance than is achievable in conventional designs.

This document is organized as follows: Section II describes the principles underlying the proposed filters, including active control and its use in capacitor-path inductance cancellation. The adaptive control techniques used to maintain high performance across operating conditions are described in Section III. Section IV presents results from a prototype coupled-magnetic filter in a dc-dc converter application. Finally, Section V concludes the paper.

## II. ACTIVE INDUCTANCE CANCELLATION CONTROL

Coupled magnetic filters can be built using two windings on a single core. Two possible implementations of such a coupled magnetic device are depicted in Fig. 2. In both configurations, each winding links flux with itself and mutually with the other winding. The mutual inductance is designed to yield the desired performance (zero shunt-path inductance) as described below.

Electromagnetic analysis of the magnetic circuit of Fig. 2(b), for example, leads to the following description [2], [3], [5]:

$$\begin{bmatrix} \lambda_1 \\ \lambda_2 \end{bmatrix} = \begin{bmatrix} \frac{N_1^2}{\mathcal{R}_{11}} + \frac{N_2^2}{\mathcal{R}_M} & \frac{N_1 \cdot N_2}{\mathcal{R}_M} \\ \frac{N_1 \cdot N_2}{\mathcal{R}_M} & \frac{N_2^2}{\mathcal{R}_{22}} + \frac{N_1^2}{\mathcal{R}_M} \end{bmatrix} \begin{bmatrix} i_1 \\ i_2 \end{bmatrix} = \begin{bmatrix} L_{11} & L_M \\ L_M & L_{22} \end{bmatrix} \begin{bmatrix} i_1 \\ i_2 \end{bmatrix} \quad (1)$$

in which  $\lambda_1$  and  $\lambda_2$  are flux linkages (the time integrals of individual coil voltage),  $i_1$  and  $i_2$  are individual coil currents,  $N_1$  and  $N_2$  are the number of turns in each coil, and  $\mathcal{R}_{11}$ ,  $\mathcal{R}_{22}$ , and  $\mathcal{R}_M$  are the self and mutual magnetic reluctances. A similar description can be realized for the center-tapped configuration of Fig. 2(a) [2]. An equivalent circuit model can be obtained from the two-port description, as illustrated in Fig. 3.

Traditionally, coupled magnetic filters of this type are designed to make inductance  $L_C$  of Fig. 3 ideally zero. An example of using a coupled magnetic element to yield a multisection filter is shown in a buck converter application in Fig. 4. The coupled magnetic element can then provide two inductances in a multisection filter such as that of Fig. 1, without contributing inductance to the shunt path. However, zeroing of the shunt-path inductance,  $L_C$ , requires very precisely-controlled coupling between the two windings, which is difficult to achieve in practice.

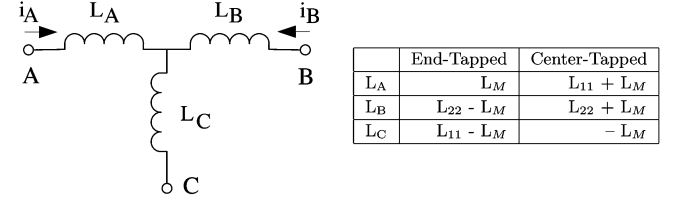


Fig. 3. Equivalent circuit "T-model" for the magnetically-coupled windings of Fig. 2.

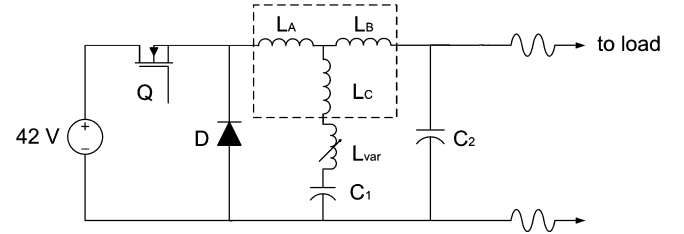


Fig. 4. Model of buck converter with a coupled magnetic filter. An external trimming inductor,  $L_{var}$ , is also shown.

Consequently, such circuits are sometimes designed to make the effective inductance,  $L_C$ , somewhat negative and an external trimming inductor is used to try to null the total shunt-path inductance [12], [13]. Even with such design tricks, inductance variations with operating conditions and part-to-part variations make it impossible to completely null the shunt-path inductance.

To fully appreciate the notion of trimming the shunt-path inductance, it is useful to revisit the magnetic circuit model (1). Energy conservation considerations dictate the following condition [18]:

$$L_M \leq \sqrt{L_{11} L_{22}} \quad (2)$$

which states that the mutual inductance between the windings must be less than or equal to the geometric mean of the two self-inductances. However, the mutual inductance may still be larger than one of the self-inductances, in which case one branch of the T-network (the  $L_C$  branch) appears to have a negative inductance. It must be stressed that this does not violate any physical laws since the inductance seen across any two terminals of the T-model is clearly positive. Thus, when  $L_C$  of Fig. 3 is made slightly negative, the trimming inductor can be used to bring the overall shunt-path inductance to zero.

Trimming the shunt-path inductance (ideally) to zero provides the performance of the two-inductor filter of Fig. 1. Because low-pass filters operate on the mismatch between the shunt- and series-path impedances, minimizing the shunt-path inductance maximizes filter performance beyond the filter cutoff frequencies (cf., the discussion of the effects of filter parasitic inductance in [1]). Approximating zero shunt-path inductance (e.g., through design of the coupled magnetics and/or addition of a trimming inductor) is thus a design strategy long associated with "zero-ripple" filters.

Unfortunately, this approach is not robust, as it is very sensitive to small material and manufacturing variations and to changes in operating conditions, such as temperature changes and flux levels. Furthermore, even in the ideal case of precise coupling, an additional limitation to high frequency filter

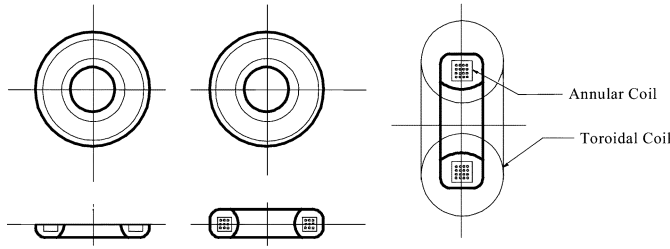


Fig. 5. Structural diagram of a cross-field reactor. One magnetic core is wound with two orthogonal windings, a toroidal coil and annular coil, which are not magnetically coupled.

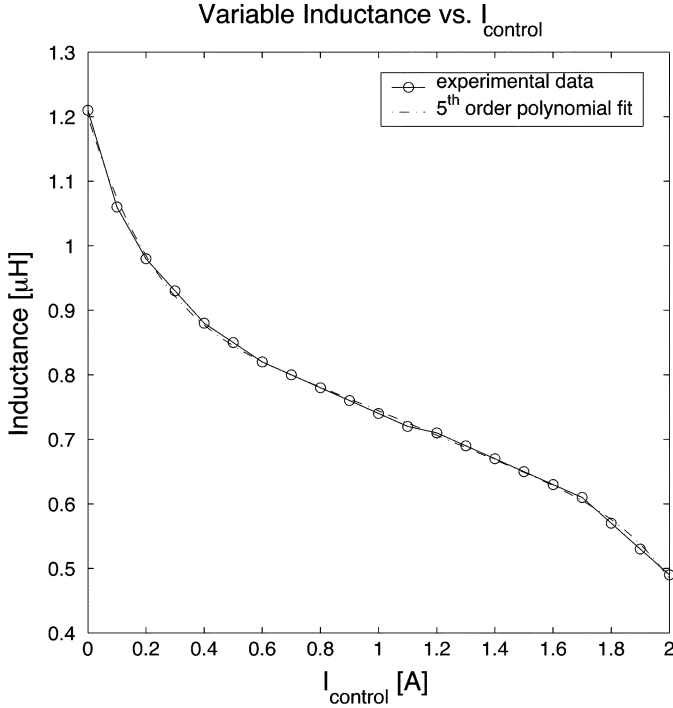


Fig. 6. Effects of varying control current on inductance using a cross-field reactor.

performance is the parasitic inductance of the shunt-path capacitor. While the effects of parasitic inductance are significant, the value of this inductance is quite small—approximately 10–50 nH for typical capacitors used in power electronics applications [2], [3], [5]. Generally, these values are well below the practical limits in trimming the shunt-path inductance.

In this paper, we introduce the use of adaptively-controlled magnetic circuits to maintain low shunt-path inductance under all operating conditions. Feedback control is used to maintain the inductance precisely at the point that optimizes attenuation performance, thereby overcoming the limitations of conventional designs. In principle, control may be achieved by adding an auxiliary winding to the coupled magnetic device, which would serve to drive part of the magnetic core a controlled amount into saturation, thereby controlling coupling [5], [15], [19]–[21]. However, for simplicity we have focused on using a separate electronically-controlled trimming inductor in the shunt path of the filter.

This electronically-controlled trimming inductor is realized as a cross-field reactor consisting of two magnetically-orthogonal sets of windings on the same core (Fig. 5). When the wind-

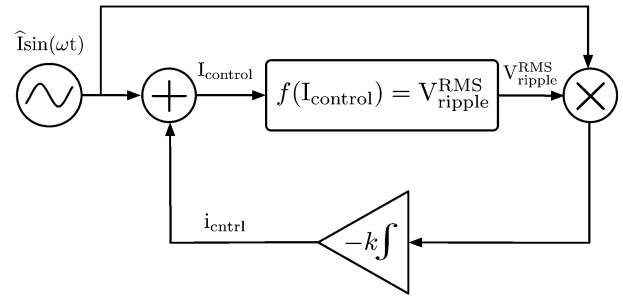


Fig. 7. Simplified closed-loop adaptive inductance tuning model.

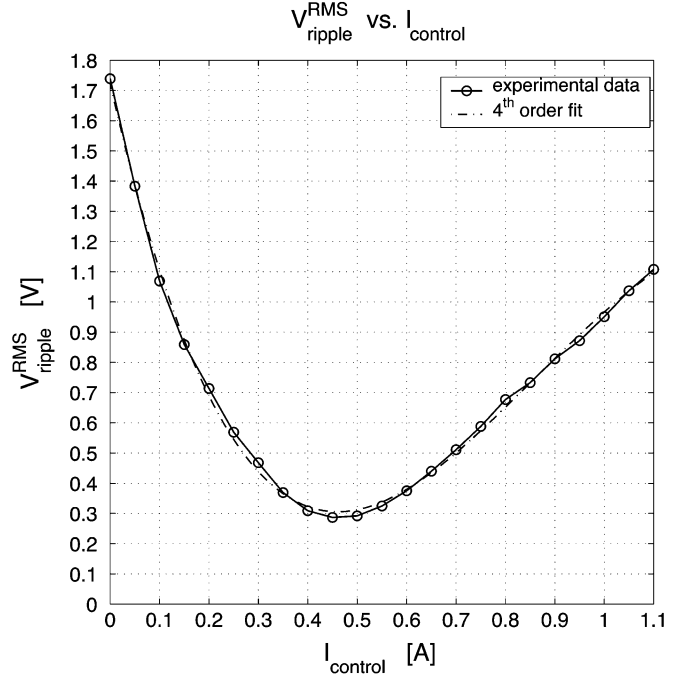


Fig. 8. Scaled  $V_{\text{RMS\_ripple}}^{\text{RMS}}$  as a function of the variable inductor control current for the prototype system (as measured at the output of AD637 of Fig. 12) and its 4th order polynomial fit. The scaling factor of 148.3 at the switching frequency results from the added gain of the differential high-pass filter stage at the input of the AD637.

ings are positioned in this way, there is no mutual magnetic coupling between them. One of the windings carries the shunt-path ripple current, while the other carries a controlled dc current. The control current is used to drive the magnetic core partly into saturation, thereby changing the permeability of the core. Effectively, this changes the inductance seen in the signal path, and the device acts as an electronically-controlled variable inductor. The measured inductance versus control current of the cross-field reactor used in our prototype system is shown in Fig. 6.

The cross-field reactor then allows us to control the overall shunt-path inductance of the filter. In this way, we are able to not only compensate for coupling mismatch of the coupled magnetic device, but to also cancel the parasitic inductance of the capacitor. Moreover, by measuring output ripple performance and placing the coupling under closed-loop control, we can maximize attenuation under all operating conditions. Experimental results demonstrating the high performance of this approach are presented in Section IV.

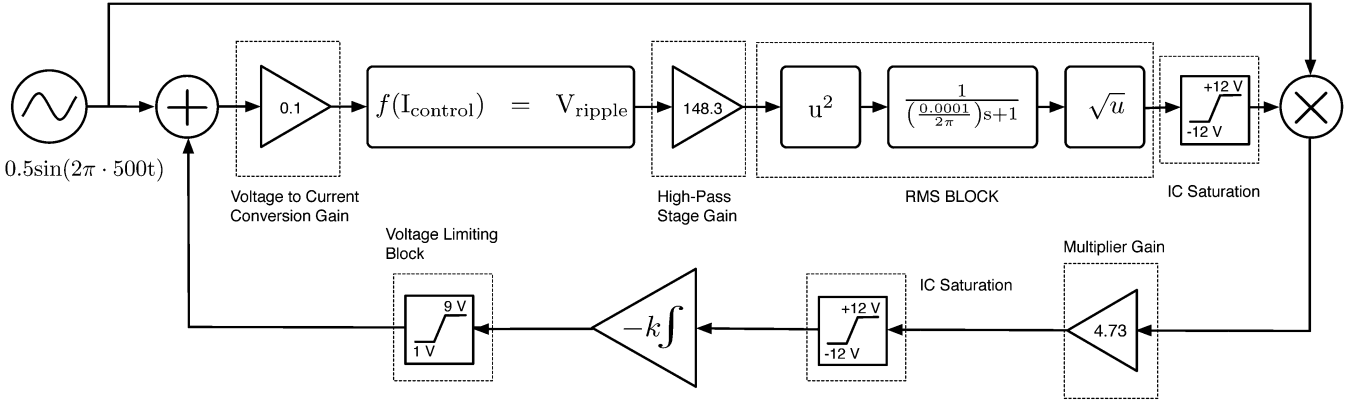


Fig. 9. Simulink model of the proposed control strategy.

### III. ADAPTIVE CONTROL METHODS

The proposed design approach uses feedback control based on output ripple to maintain good performance. The adaptive controller is presented in the context of a switching dc-dc converter application. The controller measures the root-mean-square (RMS) of the converter output ripple voltage ( $V_{\text{ripple}}^{\text{RMS}}$ ) and electronically tunes the inductance of the cross-field reactor to minimize the ripple seen at the filter output. A Lyapunov control strategy similar to those described in [8], [22]–[24] has been implemented.

The strategy employed is based on the observation that filter output ripple is minimized when the effective shunt-path inductance (e.g., through  $C_1$  in Fig. 4) is zero, and increases unimodally as the effective shunt-path inductance deviates from zero in either direction. This behavior occurs because increasing shunt-path inductance magnitude from zero reduces the impedance mismatch between the series and shunt filter paths (for frequencies beyond filter cutoff), thereby unimodally increasing ripple amplitude. Additionally, in systems where the uncompensated shunt-path resonance falls far below the switching frequency (e.g., approximately 80 kHz in the prototype considered here, which operates at a switching frequency of 400 kHz), the adaptive tuning will always yield unimodal behavior. In this case, tuning toward zero shunt-path inductance monotonically improves attenuation at all frequencies of interest, while overtuning monotonically reduces attenuation at all frequencies of interest (cf., Fig. 9 in [3]). Simulation and experimental results both support this observation for the system considered here. Even in cases where this is not true, it may often be assumed that any narrowband attenuation of specific converter harmonic frequencies that may occur (e.g., due to a narrowband shunt-path resonance [4], [6]–[9]) will be insufficient to eliminate the unimodal relationship between the control current and the RMS ripple (which measures the sum of the squares of all ripple components). It may be concluded that a unimodal relation between the RMS ripple and the shunt-path inductance magnitude always exists for sufficiently small deviations from zero shunt-path inductance. Moreover, this relation will be sustained even for large deviations from zero shunt-path inductance with typical distributions of ripple spectral content and in cases where the untuned shunt-path resonance falls far below the switching frequency.

#### A. Control Strategy

The block diagram of Fig. 7 illustrates the basic control strategy employed. The control method is integral in nature. The controller generates a small, exogenous, low frequency sinusoidal variation in the cross-field reactor control current that controls the shunt-path inductance. This consequently results in small variations in  $V_{\text{ripple}}^{\text{RMS}}$  as the shunt-path inductance varies. The controller then correlates the changes in  $V_{\text{ripple}}^{\text{RMS}}$  with the sinusoidal variation in  $I_{\text{control}}$  by multiplying the two and integrating the product. When the average value of the product is negative,  $I_{\text{control}}$  is below the optimal operating point and the integral is driven to increase  $I_{\text{control}}$ . Conversely, when the average value of the product is positive,  $I_{\text{control}}$  is above the optimal operating point and the integral of the product drives  $I_{\text{control}}$  down. At the optimal operating point, the average value of the integrator input is ideally zero and the operating point is maintained.

The small sinusoidal signal is added to the negated output of the integrator and the sum is used as the control current to the variable inductor. This control strategy drives the dc component of the control current to the minimum of the  $V_{\text{ripple}}^{\text{RMS}}$  versus  $I_{\text{control}}$  function, where the integral output holds constant. The control method assumes that the RMS value of the output ripple as a function of  $I_{\text{control}}$  is unimodal in the range of interest. Experimental measurements confirm this assumption for the prototype system described in Section IV (Fig. 8).

The proposed control approach is inherently stable. Consider the local average dynamics [25] of the system in Fig. 7 over an averaging period of the sinusoidal variation:

$$\frac{d\bar{i}_{\text{ctrl}}(t)}{dt} = \frac{-k}{T} \int_{t-T}^t (\hat{I} \sin(\omega\tau) \cdot f(\hat{I} \sin(\omega\tau) + i_{\text{ctrl}}(\tau)) d\tau). \quad (3)$$

Observing the function  $f(\bar{i}_{\text{ctrl}}(t)) = V_{\text{ripple}}^{\text{RMS}}$  of Fig. 8 and the control function of (3), it is evident that at the minimum of  $f, (d\bar{i}_{\text{ctrl}}(t)/dt)$  tends to zero. Thus, the minimum of the  $V_{\text{ripple}}^{\text{RMS}}$  versus  $(\bar{i}_{\text{ctrl}}(t))$  function,  $\hat{i}_{\text{ctrl}}$ , is an equilibrium point of the system. Taking the (local average) output of the integrator as the state variable of interest, the function  $f$  of Fig. 8 is a Lyapunov function [26] of the system. The response of the system is determined by the gain  $k$ , but must be kept

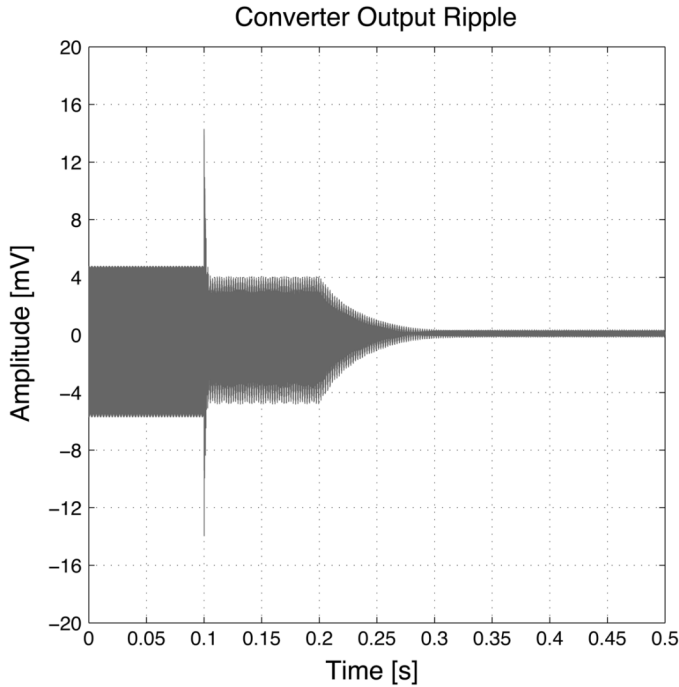


Fig. 10. Simulated transient performance of the converter output ripple as active tuning is enabled at time 0.1 s.

sufficiently slow that the dynamics of the RMS calculation may be neglected.

### B. Simulation

To validate the efficacy of the control strategy, a time domain simulation of the approach was implemented in Simulink (Mathworks, Inc., Cambridge, MA) as shown in Fig. 9. A simplified average state-space model was developed for the buck converter (described more fully in Section IV), and is represented by the  $f(I_{\text{control}}) = V_{\text{ripple}}$  block. The effects of varying the control current on the value of the variable inductance were determined empirically and modeled with a close-fitting fifth-order polynomial (Fig. 6). Transfer function blocks reflecting the dynamics and characteristics of circuit components were derived for the controller. The model was then used to assess the dynamic performance of the controller. Details of this model may be found in [27]. The converter was first allowed to reach steady state, at which point the adaptive tuning was enabled at time  $t = 0.1$  s. The transient behavior of the control current and the converter output ripple are depicted in Figs. 10 and 11.

Simulation results indicate that the proposed active tuning control method exhibits good static and dynamic behavior. A factor of 20 reduction is predicted for the converter output ripple (Fig. 10) when  $I_{\text{control}}$  reaches its dc steady state value of 0.53 A within approximately 250 ms of the control circuitry activation at 100 ms (Fig. 11).

### C. Controller Implementation

In practice, the controller is implemented on a printed circuit board (PCB) using standard circuit components, as illustrated in Fig. 12. The blocks of Fig. 9 are implemented as follows: the sinusoidal variation is implemented using an XR2206 monolithic function generator. The frequency of the sinusoid is chosen to be low compared to the RMS averaging frequency, and the

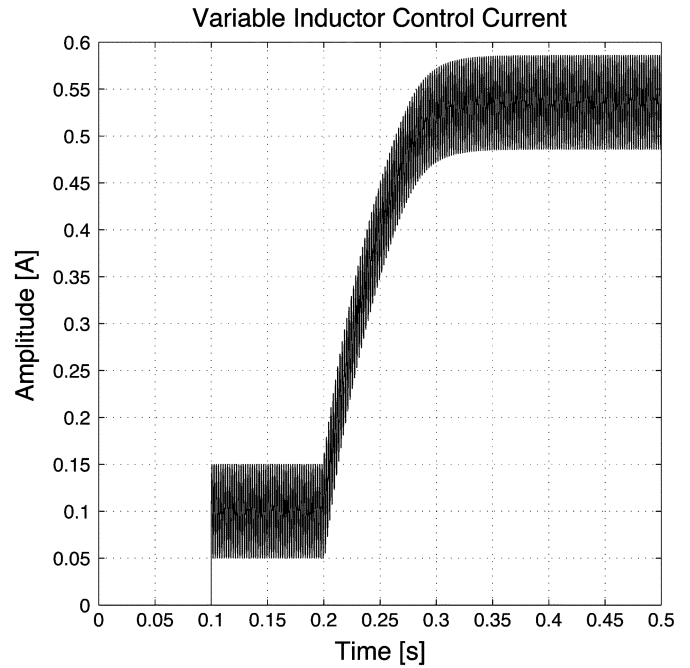


Fig. 11. Simulated transient performance of the variable inductor control current as active tuning is enabled at time 0.1 s.

amplitude is chosen to be low but sufficiently high to sweep the  $V_{\text{ripple}}^{\text{RMS}}$  versus  $I_{\text{control}}$  function. An AD637 RMS-to-dc converter is used for the RMS block and an AD633 multiplier for the product block. Addition, integration, buffering, and voltage to current conversion are performed using the LF347 quad operational amplifier. The variable inductor control current is provided using a TIP29C NPN power bipolar transistor. A zener diode and the LM317 adjustable voltage regulator serve to constrain the voltage at the output of the integrator in the range of 1–9 V, corresponding to an appropriate control current range. Finally, a differential high-pass stage is added using two LM6361 wide bandwidth operational amplifiers to provide additional gain and to decouple the dc component of the output from the control circuitry.

## IV. PROTOTYPE SYSTEM

In this section, we validate the proposed design strategy in a buck converter having a coupled-magnetic output filter, as illustrated in Figs. 13 and 14 and Tables I and II. The converter operates under averaged current-mode control at a switching frequency of 400 kHz, and is designed to regulate the output at 14 V from a nominal input of 42 V; this conversion function is relevant to some emerging automotive applications, for example [28]. The converter is designed to support a load range of 16 W to 65 W.

In addition to the coupled-magnetic element (described in detail below), the output filter comprises capacitors  $C_1$  and  $C_2$ .  $C_1$  is implemented as a 10- $\mu\text{F}$  high-ripple, low-inductance film capacitor (ITW Paktron 106K050CS4).  $C_2$  is implemented as a parallel combination of a 20- $\mu\text{F}$  polypropylene capacitor (Cornell-Dubilier 935C1W20K), a 2200- $\mu\text{F}$  electrolytic capacitor (50 V,  $R_{\text{ESR}} = 0.040 \Omega$ ), and a 0.1- $\mu\text{F}$  ceramic capacitor. Additionally, a large 27 mF electrolytic capacitor was placed in parallel with the load (physically away from the converter output).

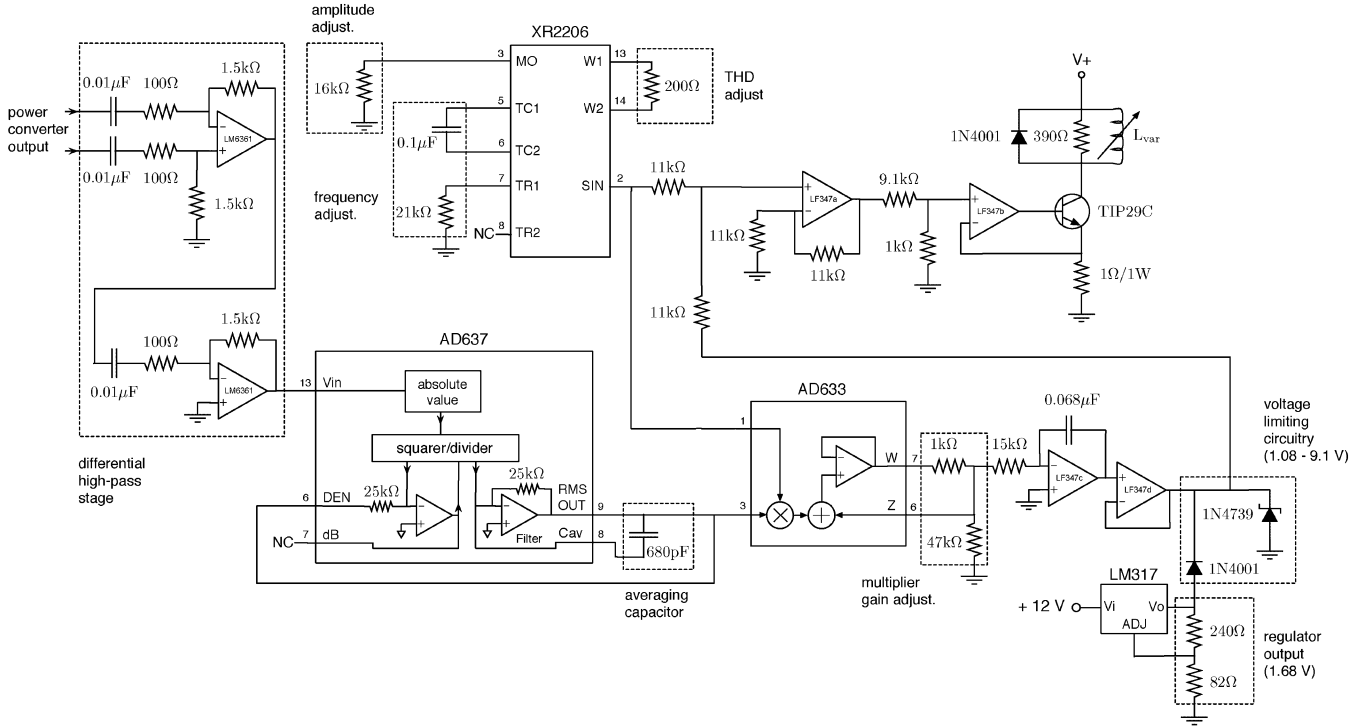


Fig. 12. Schematic of the control board circuitry.

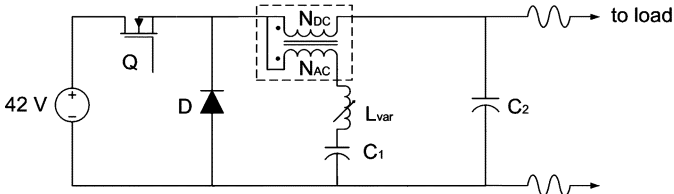


Fig. 13. Circuit schematic of the buck converter and output filter.

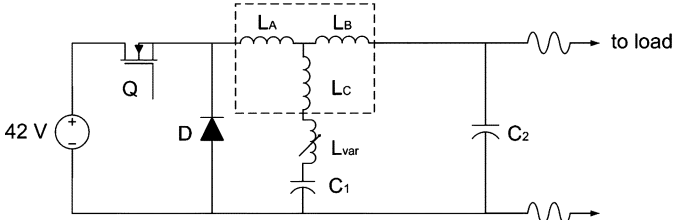


Fig. 14. Model of buck converter and coupled-magnetic filter.

TABLE I  
DEVICE PARAMETERS FOR THE BUCK CONVERTER OF  
FIG. 14 (MAGNETICS ARE DETAILED IN TABLE II)

C <sub>1</sub>	10 $\mu$ F	ITW Paktron 106K050CS4
C <sub>2</sub> (parallel combination)	20 $\mu$ F 2200 $\mu$ F 0.1 $\mu$ F	Cornell-Dubilier 935C1W20K 100V, Polypropylene Electrolytic, 50 V (R <sub>ESR</sub> = 0.040 $\Omega$ ) Ceramic
Q	IRF1010E	N-Channel Power Mosfet
D	MUR3020WT	Common Cathode Diode

TABLE II  
DEVICE PARAMETERS FOR THE COMPARISON OF THE THREE FILTER  
TOPOLOGIES USING THE BUCK CONVERTER OF FIG. 14

Magnetics	Inductor Filter	"Zero-Ripple" Filter	Tuned Coupled Magnetic Filter
Construction	RM10/I, A315 3F3 Core 5 Turns	RM10/I, A315 3F3 Core 5:5 Turns	RM10/I, A315 3F3 Core 5:4 Turns
L <sub>A</sub>	8.04 $\mu$ H	7.70 $\mu$ H	6.13 $\mu$ H
L <sub>B</sub>	0 $\mu$ H	0.34 $\mu$ H	1.67 $\mu$ H
L <sub>C</sub>	0 $\mu$ H	0.17 $\mu$ H	- 0.82 $\mu$ H

This was done to represent the behavior of the battery that would be present in an automobile, for example, or the hold-up capacitor that appears in many applications. Because this capacitor is in parallel with the remote load, away from the actual converter output, it does not have a significant impact on the converter output switching ripple or serve to attenuate EMI. The capacitor does, however, provide low-frequency voltage holdup during load transients.

#### A. Adaptive Coupled-Magnetic Design

The end-tapped configuration of the coupled-magnetic device [Fig. 2(b)] was chosen and implemented with the two windings separated on the bobbin in such a way as to minimize the capacitance across them. One winding was wound on the top half, while the other was wound on the bottom half of the bobbin. An RM10/I A315 3F3 core was used to construct the coupled-magnetic device. A turns ratio of 5:4 [ $N_{DC}:N_{AC}$  in Fig. 13 or  $N_2:N_1$  in Fig. 2(b)] was used. For the dc winding, AWG 12 wire was used, and for the ac winding, Litz 175/40 wire was used. Litz

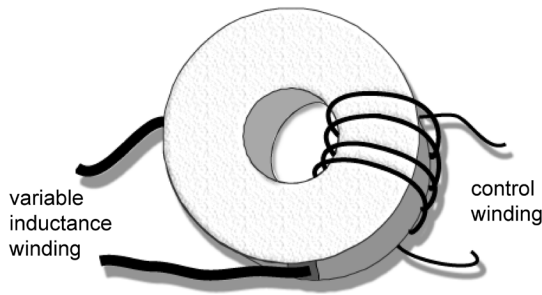


Fig. 15. Variable inductor.

wire is useful for minimizing the ac resistance of the capacitor path, but it is not as important as it would be in a resonant filter system [15]. The resulting coupled-magnetic device parameters are listed in column 4 of Table II. Experimental measurements indicate that the windings appear inductive for frequencies up to  $\sim 11$  MHz.

The variable inductor is approximately an order of magnitude smaller than the main coupled-magnetic element. It was designed such that its tunable range captured the inductance to be cancelled, namely the sum of the shunt-path inductance of the coupled-magnetic device and the parasitic inductance of the shunt-path capacitor. Construction of the variable inductor was as follows: two turns of the coupled-magnetic ac winding were wound conventionally on the bobbin of a P14/8 A315 3F3 core. The control winding was constructed using 77 turns of AWG 28 wire wound through the center-post hole of the core (orthogonally to the inductance winding), as illustrated in Fig. 15. In order to reduce the control current required to partially saturate the variable inductor core, a high number of turns for the control winding was used.

The maximum power dissipation in the control winding over the regulated range (for 0.96 A maximum current) was low (1.5 W), corresponding to 2.3% of maximum output power. In practice, the control current required to achieve the desired operation was far lower ( $\sim 0.4 - 0.5$  A), corresponding to control winding dissipation of less than 1% of maximum converter output power. This was deemed acceptable for the purposes of the prototype design.

For experimental simplicity, voltage  $V^+$  in Fig. 12 was fed from a 12-V supply, though in principle, it could have been provided by a far lower supply voltage (less than 3 V), keeping total dissipation to at most a few percent of maximum output power. Moreover, supplying the winding through improved circuitry could yield dissipation as low as the maximum control winding dissipation for the same control range. In systems where such a loss is deemed too high, a more rigorous selection of the required control range and/or providing more winding area for the control windings could reduce this dissipation to far lower levels. Finally, we note that it is Ampere-turns that govern the inductance control; a lower absolute control current (at higher drive voltage) could be obtained by rewinding the control winding with more turns of smaller gauge wire. We conclude, therefore, that for many applications control loss is not a severe limiting factor.

### B. Conventional Filter Designs

For comparison purposes, two conventional designs have also been implemented. To provide an even comparison, the same magnetic core type was utilized in each case with similar values

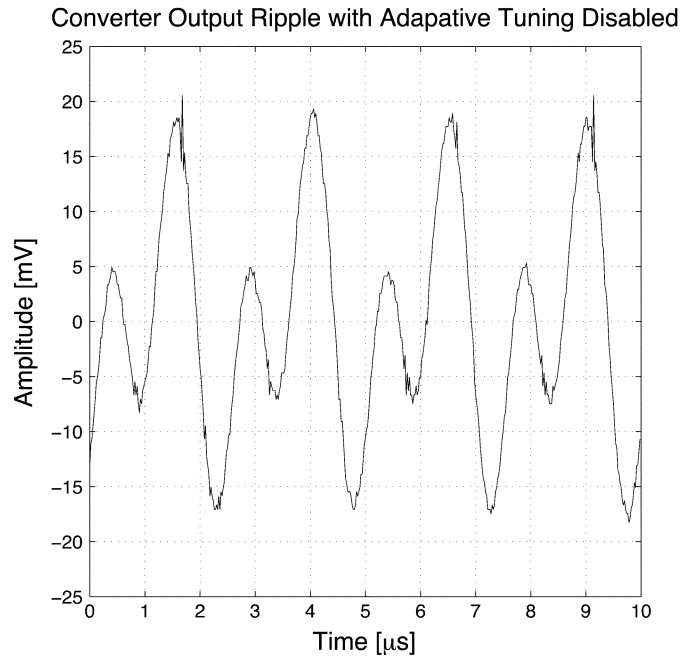


Fig. 16. Measured converter output ripple using the adaptive coupled-magnetic filter with adaptive inductance cancellation disabled. Note the scale of 5 mV/division.

for total series-path inductance [ $L_A + L_B$  in Fig. 14 or  $L_{22}$  in Fig. 2(b)]. The characteristics of all three magnetic component designs are shown in Table II.

The first conventional design is a standard buck converter inductor without coupled magnetics. In this implementation, capacitor  $C_1$  appears in parallel with  $C_2$  (reducing the order of the filter), but there is no coupling sensitivity in the design. The second conventional design is a “zero-ripple” design in which the shunt-path inductance ( $L_C$  in Fig. 14) is designed to be as close to zero as possible without external trimming. It was found that a 5:5 turns ratio [ $N_{DC}:N_{AC}$  in Fig. 13 or  $N_2:N_1$  in Fig. 2(b)] provided an effective shunt-path inductance of approximately 170 nH under low flux conditions, yielding the best approximation to a “zero-ripple” design within the overall design requirements. The capacitors  $C_1$  and  $C_2$  are realized in the same manner as in the adaptive design described in the previous section.

### C. Experimental Results for Adaptive Cancellation

The tuning method was implemented using the adaptive coupled-magnetic device described above. Time and frequency domain measurements were performed for the converter operating at 35% of maximum load ( $R_L = 8 \Omega$ ) both with adaptive inductance cancellation disabled and enabled. All time domain experimental measurements were bandwidth limited to 20 MHz, though this was not seen to have a significant impact on the results. Figs. 16 and 17 illustrate a reduction of greater than a factor of five in the peak-to-peak output ripple amplitude when active tuning is enabled.

Measurements were also made of the spectra of the output ripple with adaptive cancellation disabled and enabled using an Agilent 4395A Network/Spectrum/Impedance Analyzer with an Agilent 1141A ac-coupled differential probe. Results reflect



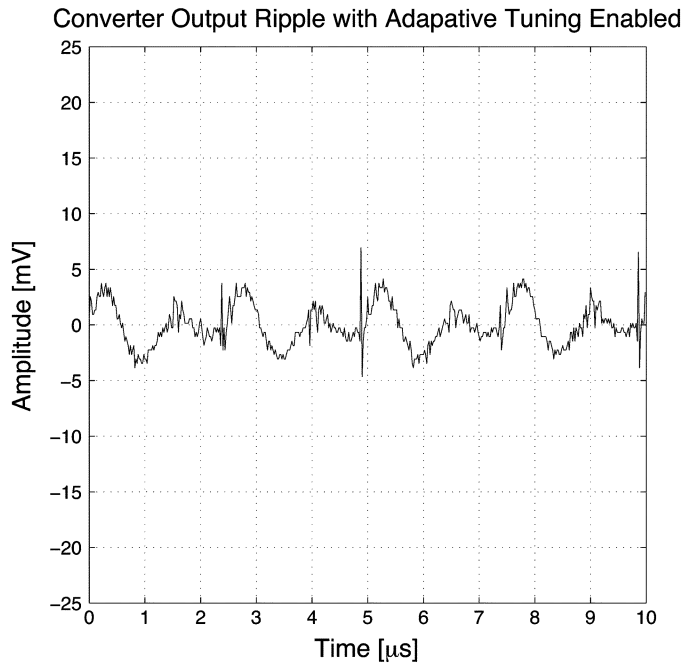


Fig. 17. Measured converter output ripple using the adaptive coupled-magnetic filter with adaptive inductance cancellation enabled. Note the scale of 5 mV/division.

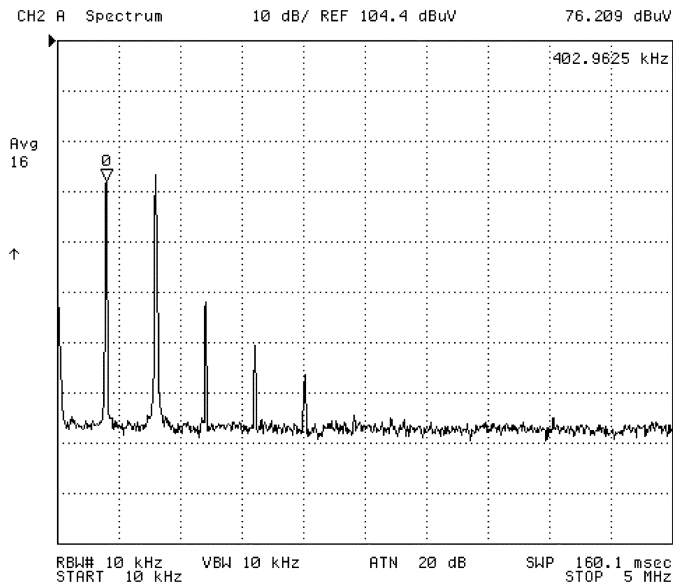


Fig. 18. Measured spectrum of the converter output ripple using the adaptive coupled-magnetic filter with active tuning disabled. The horizontal scale is linear from 10 kHz to 5 MHz, and the vertical scale is 10 dB/div referenced at 104.4 dBμV at the top of the scale.

an improvement of approximately 16 dBμV for the first two harmonic components (Figs. 18 and 19). These components are the main contributors to time-domain ripple, and the measured results are consistent with the peak-to-peak values observed in the time domain.

The transient performance of the adaptive inductance cancellation method was also experimentally assessed. To test this, the output of the converter was allowed to reach steady state. Once steady state was reached, adaptive cancellation was enabled by turning on the power supply to the control circuitry,

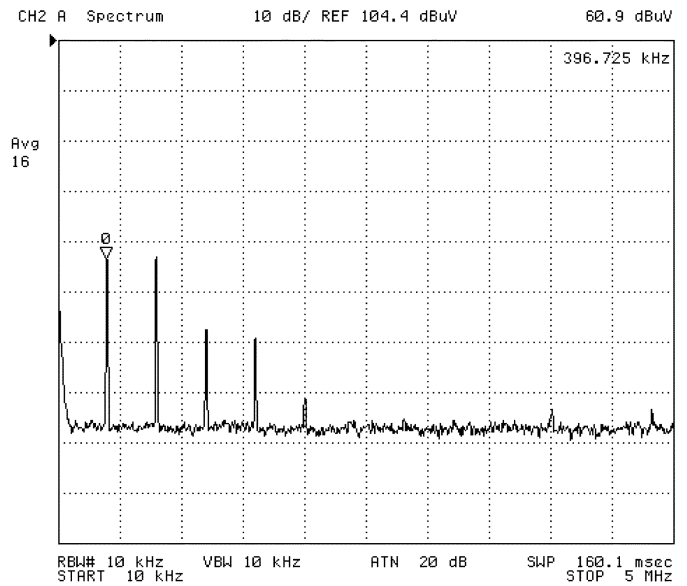


Fig. 19. Measured spectrum of the converter output ripple using the adaptive coupled-magnetic filter with active tuning enabled. The horizontal scale is linear from 10 kHz to 5 MHz, and the vertical scale is 10 dB/div referenced at 104.4 dBμV at the top of the scale.

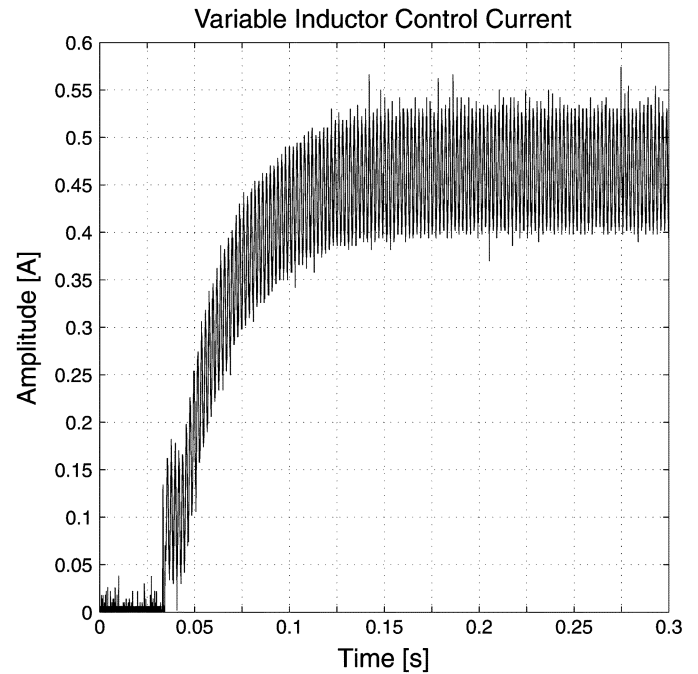


Fig. 20. Measured transient performance of the variable inductor control current as active tuning is enabled.

and experimental measurements for the variable inductor control current and the converter output ripple were made. As illustrated in Figs. 20 and 21, the maximum reduction in output ripple amplitude is reached after approximately 100 ms when the dc component of  $I_{\text{control}}$  reaches its steady state value of 0.49 A and remains stable. The experimental results illustrate that the adaptive control is stable and effective at reducing the output ripple.

The experimental results match the simulation predictions within the limits of the model. The minor differences between the simulation predictions and experiment are within the bounds

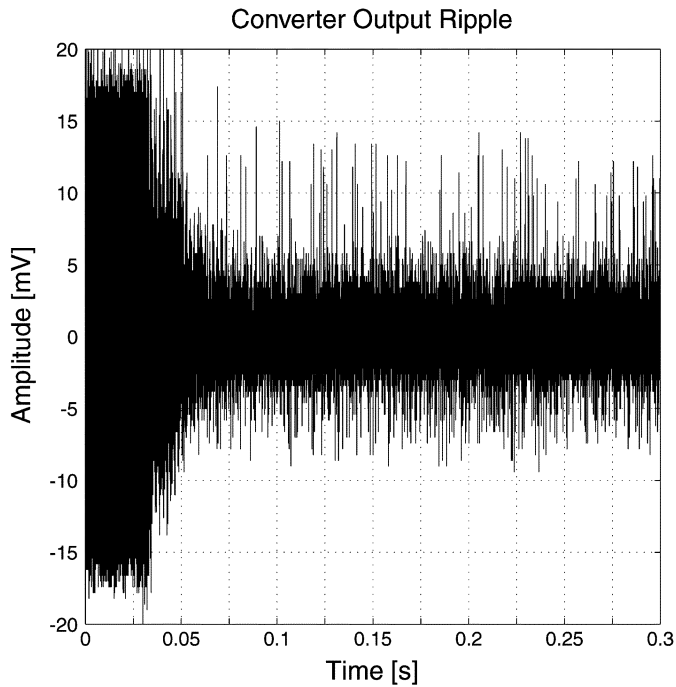


Fig. 21. Measured transient performance of the converter output ripple as active tuning is enabled. The measured signal is highly undersampled.

expected due to modeling simplifications. For example, the optimal value of  $I_{\text{control}}$  is reached faster than is predicted by simulation (Figs. 10 and 11). Likewise, the predicted reduction in ripple, as well as the peak-to-peak ripple values predicted by simulation are lower than those measured experimentally. This is due to the fact that the simplified state-space model that was used for the converter contains only the essential components that influence the overall converter dynamics and neglects some of the parasitics present in the system. Nevertheless, it can be seen from the experimental results that the adaptive system is stable and effective at reducing power converter output ripple.

The performance of the adaptive tuning method was also assessed in the presence of a slow-varying load (Figs. 22 and 23). The converter load consists of a parallel combination of a resistor and a 27-mF hold-up capacitor. Load transient measurements were performed for load steps corresponding to 35%–70% of maximum output power. A maximum 3% fluctuation in the converter output voltage is observed for this load transient (Fig. 22). Additionally, experimental results under maximum load step conditions show a limited ( $< 5\%$ ) transient in output voltage. Observing the (undersampled) switching ripple during the transient by ac coupling the output voltage measurement, it is seen that the adaptive control is able to provide the desired ripple cancellation without undesired interactions with the output voltage control.

#### D. Comparison With Conventional Filter Designs

It is also informative to compare the coupled magnetic filter with adaptive inductance cancellation to the conventional designs described in Section IV-B. Figs. 24 and 25 show the time and frequency domain ripple measurements for the converter using a conventional inductor. Comparing these results to those of Figs. 17 and 19, it can be seen that the coupled-magnetic

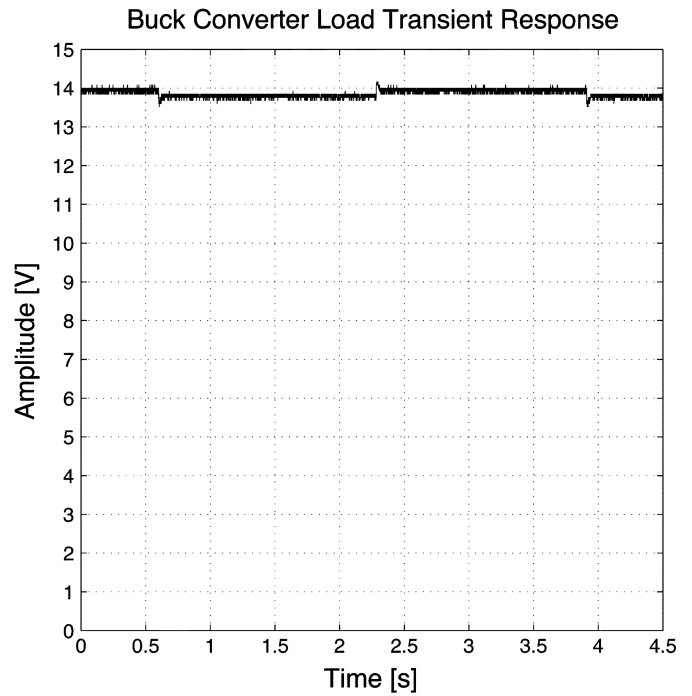


Fig. 22. Measured converter output voltage during load step transients between 35%–70% of maximum power.

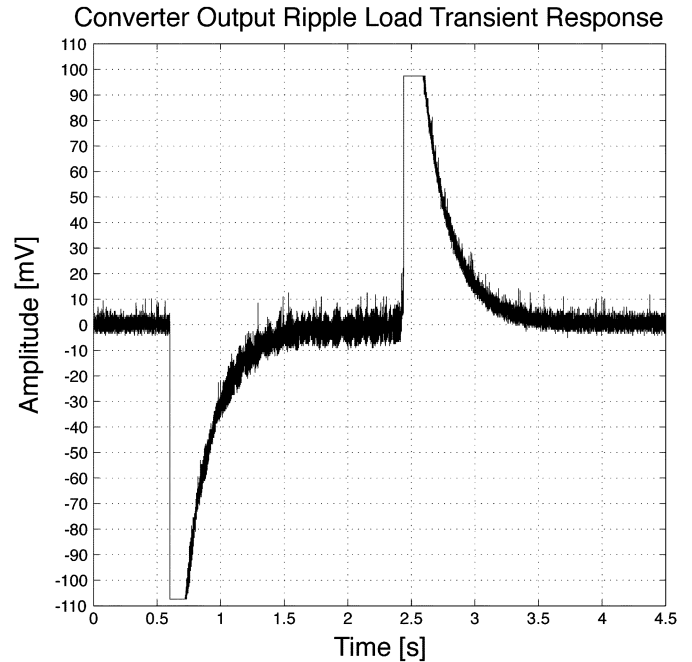


Fig. 23. Measured converter output ripple during load step transients between 35%–70% of maximum power. The measured signal is highly undersampled. The observed saturation and settling time are due to the measurement method. The observed saturation in the transient is due to the amplifier saturation in the ripple measurement. The ripple is measured by ac coupling of the output voltage measurement, and the apparent duration of the transients is due to the ac coupling. It can be seen that the active control adjusts within the expected time period.

filter with adaptive inductance cancellation provides more than a factor of 10 ( $> 20$  dB) improvement in output ripple performance as compared to a buck converter with the same passive component size.

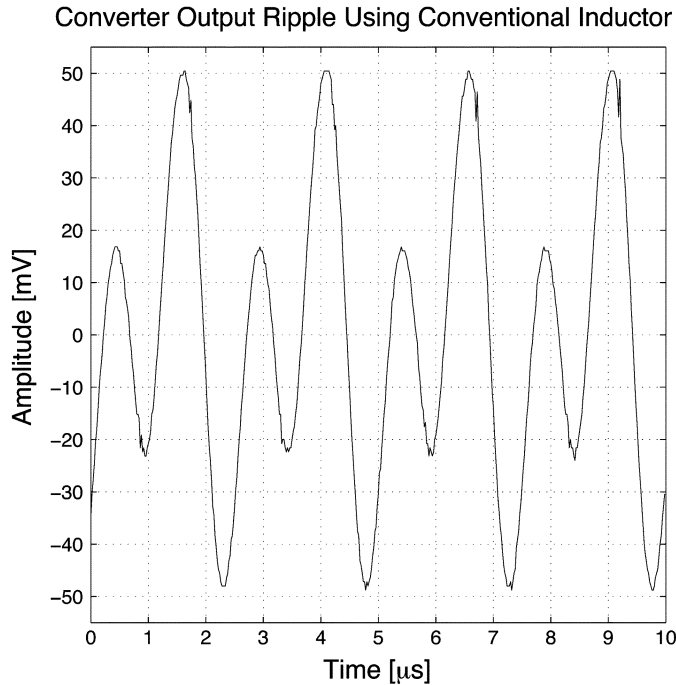


Fig. 24. Measured converter output ripple using a conventional inductor filter. Note the scale of 10 mV/division.

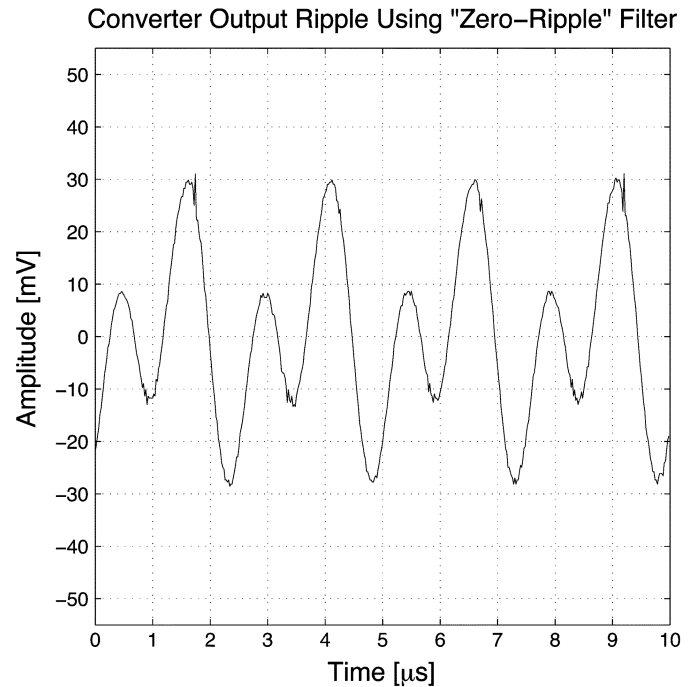


Fig. 26. Measured converter output using a "zero-ripple" filter. Note the scale of 10 mV/division.

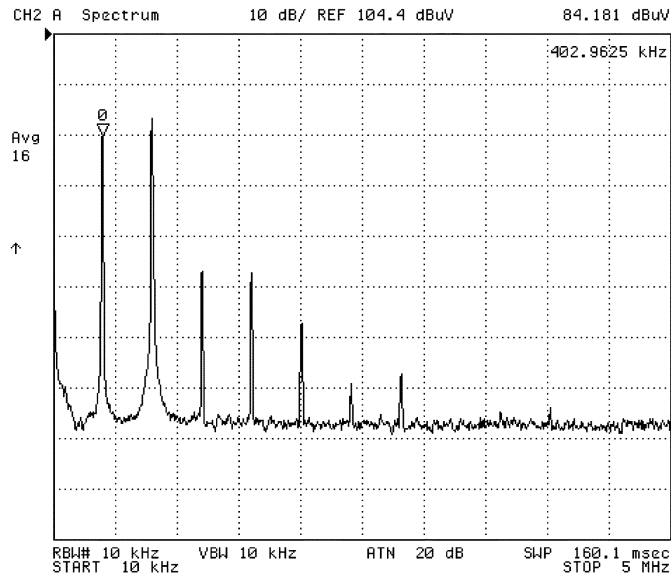


Fig. 25. Measured spectrum of the converter output ripple using a conventional inductor filter. The horizontal scale is linear from 10 kHz to 5 MHz, and the vertical scale is 10 dB/div referenced at 104.4 dB $\mu$ V at the top of the scale.

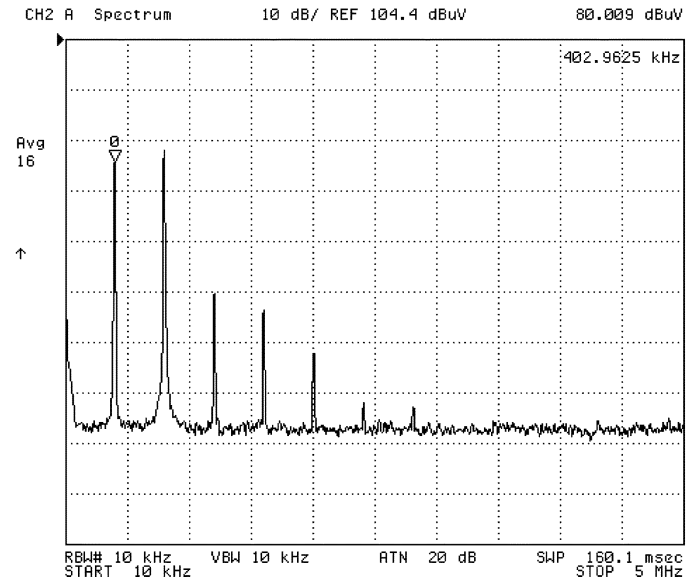


Fig. 27. Measured spectrum of the converter output ripple using a "zero-ripple" filter. The horizontal scale is linear from 10 kHz to 5 MHz, and the vertical scale is 10 dB/div referenced at 104.4 dB $\mu$ V at the top of the scale.

It is also interesting to compare these results to the "best designed" "zero-ripple" filter, in which "shunt-path" inductance is minimized. Results from this design are shown in Figs. 26 and 27. It can be seen that the performance of this design is substantially better than that of the converter without coupled magnetics, but falls far short of those achieved with the adaptive inductance cancellation. In fact, performance of this filter (with minimized shunt-path inductance) is slightly worse than the performance of the coupled magnetics design with adaptive cancellation disabled. This is attributed to the fact that despite having a higher

shunt-path impedance (without active cancellation), inductance  $L_B$  of Fig. 14 is higher in the design for active cancellation, thereby providing a better second filter stage. Ultimately, it may be concluded that the ripple performance of the coupled-magnetic filter with inductance cancellation is a factor of more than five better than any of the other options explored, and provides a much higher robustness to manufacturing and operating point variations owing to its use of closed-loop control.

Finally, the performance of the two conventional designs and of the coupled-magnetic filter with adaptive inductance cancel-

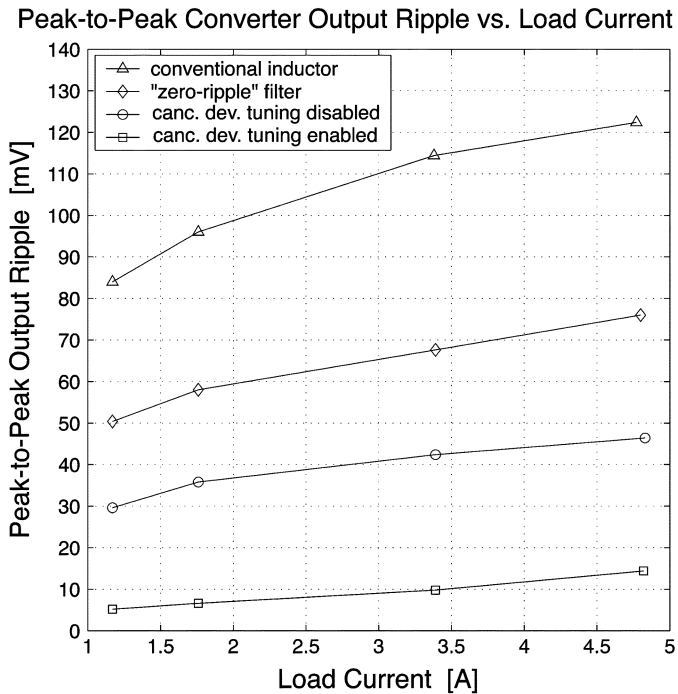


Fig. 28. Comparison of measured peak-to-peak converter output ripple versus load current for four output filter designs: the adaptive coupled-magnetic with active tuning enabled, with tuning disabled, the “zero-ripple” filter, and a conventional inductor.

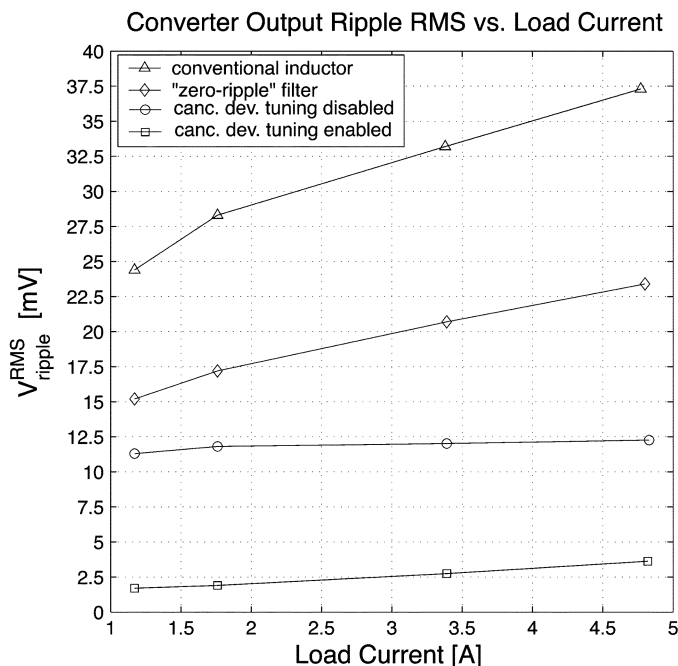


Fig. 29. Comparison of measured converter output RMS versus load current for four output filter designs: the adaptive coupled-magnetic with active tuning enabled, with tuning disabled, the “zero-ripple” filter, and a conventional inductor.

lation enabled and disabled is compared across varying load conditions. Figs. 28 and 29 illustrate the converter output ripple and output ripple RMS for each type of filter as the load current is increased from minimum to maximum. It can be seen that the coupled-magnetic filter with adaptive inductance cancellation provides the greatest ripple attenuation across the specified

prototype buck converter load range. At the maximum output power, the adaptive coupled-magnetic filter demonstrates more than a factor of three improvement over the coupled-magnetic filter with tuning disabled, a factor of five improvement over the “zero-ripple” filter, and more than a factor of eight improvement over the conventional inductor, both in the peak-to-peak converter output ripple and the output ripple RMS.

It can be seen in Figs. 28 and 29 that in each filter type the peak-to-peak and RMS ripple increases with load current. This change can be attributed to a reduction in the permeability of the main filter magnetics as flux levels increase, which reduces filter attenuation. This effect is smallest in absolute terms, but largest in percentage terms, for the coupled-magnetic filter with adaptive inductance cancellation. Further increase in load current rapidly degrades the performance of the filter with active cancellation, as the small cross-field reactor used to adapt the filter begins to saturate for high ripple currents. Nonetheless, the adaptive coupled-magnetic filter provides the best ripple attenuation over the entire rated load range. Changes in performance of all the filters with the load can in principle be amended by designing the output filter magnetics to present smaller changes in inductance over the load range.

## V. CONCLUSION

Conventional filter circuits suffer from a number of limitations, including performance degradation due to capacitor parasitic inductance and the size and cost of magnetic elements. Coupled-magnetic filters have been developed that provide increased filter order with a single magnetic component, but also suffer from parasitic inductance in the filter shunt path due to imperfectly-controlled coupling of the magnetics. This paper introduces coupled-magnetic filters with adaptive inductance cancellation control. The proposed approach provides a robust method of increasing filter order and canceling the effects of parasitic inductance without a substantial increase in filter size and cost. Using this method, one can either achieve greatly improved EMI/ripple performance for a similar magnetics size (as demonstrated here) or potentially reduce magnetics size for a given level of ripple performance. Simulation and experimental results confirm the high performance of the proposed approach in a dc-dc power converter application. It may be concluded that the proposed approach offers greatly improved ripple attenuation and robustness in circuits employing coupled-magnetic filters, and has merit where these advantages justify the needed control circuitry. In particular, we anticipate that the proposed approach will find best use in high power applications and in very low ripple applications where the size and cost of the required control circuitry is small in comparison to the benefits to the filter design.

## REFERENCES

- [1] T. K. Phelps and W. S. Tate, “Optimizing passive input filter design,” in *Proc. 6th Nat. Solid-State Power Conv. Conf.*, May 1979, pp. G1-1–G1-10.
- [2] T. C. Neugebauer, J. W. Phinney, and D. J. Perreault, “Filters and components with inductance cancellation,” *IEEE Trans. Ind. Appl.*, vol. 40, no. 2, pp. 483–491, Mar./Apr. 2004.
- [3] T. C. Neugebauer and D. J. Perreault, “Filters with inductance cancellation using printed circuit board transformers,” *IEEE Trans. Power Electron.*, vol. 19, no. 3, pp. 591–601, May 2004.

- [4] P. T. Krein, *Elements of Power Electronics*. New York: Oxford Univ. Press, 1998, pp. 381–392.
- [5] D. J. Perreault, J. W. Phinney, and T. C. Neugebauer, "Filter Having Parasitic Inductance Cancellation," U.S. Patent 6 937 115 B2, Aug. 30, 2005.
- [6] G. B. Crouse, "Electrical Filter," U.S. Patent 1 920 948, Aug. 1, 1933.
- [7] S. Feng, W. A. Sander, and T. G. Wilson, "Small-capacitance nondissipative ripple filters for dc supplies," *IEEE Trans. Magn.*, vol. MAG-6, no. 1, pp. 137–142, Mar. 1970.
- [8] R. Balog and P. T. Krein, "Automatic tuning of coupled inductor filters," in *Proc. IEEE Power Electron. Spec. Conf.*, 2002, pp. 591–596.
- [9] J. Phinney and D. J. Perreault, "Filters with active tuning for power applications," *IEEE Trans. Power Electron.*, vol. 18, no. 2, pp. 636–647, Mar. 2003.
- [10] D. C. Hamill and P. T. Krein, "A 'zero' ripple technique applicable to any dc converter," in *Proc. IEEE Power Electron. Spec. Conf.*, Jun. 1999, pp. 1165–1171.
- [11] J. W. Kolar, H. Sree, N. Mohan, and F. C. Zach, "Novel aspects of an application of 'zero'-ripple techniques to basic converter topologies," in *Proc. IEEE Power Electron. Spec. Conf.*, Jun. 1997, pp. 796–803.
- [12] R. P. Severns and G. E. Bloom, *Modern DC-to-DC Switchmode Power Converter Circuits*. New York: Van Nostrand Reinhold, 1985, ch. 12.
- [13] G. E. Bloom and R. Severns, "The generalized use of integrated magnetics and zero-ripple techniques in switchmode power converters," in *Proc. IEEE Power Electron. Spec. Conf.*, 1984, pp. 15–33.
- [14] S. Senini and P. J. Wolfs, "The coupled inductor filter: Analysis and design for ac systems," *IEEE Trans. Ind. Electron.*, vol. 45, no. 4, pp. 574–578, Aug. 1998.
- [15] J. W. Phinney, "Filters with Active Tuning for Power Applications," S.M. thesis, Dept. Elect. Eng. & Comp. Sci., Mass. Inst. Technol., Cambridge, May 2001.
- [16] ITW Paktron, "Capstick Capacitor Type CS4, CS6 Datasheet," Doc. Part 106K050CS4, Dec. 2005 [Online]. Available: <http://www.paktron.com>
- [17] H. W. Ott, *Noise Reduction Techniques in Electronic Systems*. New York: Wiley, 1988, pp. 137–143.
- [18] D. J. Perreault, "OpenCourseWare 6.334 Power Electronics, Spring 2003 Lecture Notes: Introduction to Magnetics," MIT, Dec. 2005, p. 45A [Online]. Available: <http://ocw.mit.edu/NR/rdonlyres/Electrical-Engineering-and-Computer-Science/6-334Spring2003/80CB0C7E-BD5D-4C60-A16E-6640839AC85D/0/PG3648D.pdf>
- [19] R. Hertz and H. Buelteman, "The application of perpendicularly superposed magnetic fields," *AIEE Trans.*, vol. 74, pt. I, pp. 655–660, Nov. 1955.
- [20] H. J. McCreary, "The magnetic cross valve," *AIEE Trans.*, vol. 70, pt. II, pp. 1868–1875, 1951.
- [21] F. J. Beck and J. M. Kelly, "Magnetization in perpendicularly superposed direct and alternating fields," *J. Appl. Phys.*, vol. 19, pp. 551–562, Jun. 1948.
- [22] D. L. Logue, "Power Electronic Building Block Applications in Optimization, Control, and Simulation," Ph.D. dissertation, Dept. of Elect. Comp. Eng., Univ. of Illinois at Urbana-Champaign, Urbana, Oct. 2000.
- [23] D. L. Logue and P. T. Krein, "Optimization of power electronic systems using ripple correlation control: A Dynamic programming approach," in *Proc. IEEE Power Electron. Spec. Conf.*, 2001, pp. 459–464.
- [24] P. Midya and P. T. Krein, "Feed-forward active filter for output ripple cancellation," *Int. J. Electron.*, vol. 77, no. 5, pp. 805–818, Jun. 1994.
- [25] J. G. Kassakian, M. F. Schlecht, and G. C. Verghese, *Principles of Power Electronics*. New York: Addison-Wesley, 1991, ch. 11–12.
- [26] D. G. Luenberger, *Introduction to Dynamic Systems*. New York: Wiley, 1979.
- [27] D. S. Lyman, "Coupled-Magnetic Filters with Adaptive Inductance Cancellation," M.Eng. thesis, Department of Elect. Eng. Comp. Sci., Mass. Inst. of Technol., Cambridge, MA, Jun. 2005.
- [28] T. C. Neugebauer and D. J. Perreault, "Computer-aided design of DC/DC converters for automotive applications," *IEEE Trans. Power Electron.*, vol. 18, no. 3, pp. 775–783, May 2003.



**Daria S. Lyman** received the S.B. and M.Eng. degrees in electrical engineering from the Massachusetts Institute of Technology, Cambridge, in 2003 and 2005, respectively.



**Timothy C. Neugebauer** (M'05) received the B.S. degree in electrical engineering from Union College, Schenectady, NY, in 1997 and the M.S. and Ph.D. degrees from the Massachusetts Institute of Technology, Cambridge, in 1999 and 2004, respectively.

He is currently with Draper Laboratories, Cambridge.



**David J. Perreault** (S'91–M'97–SM'06) received the B.S. degree from Boston University, Boston, MA, in 1989, and the S.M. and Ph.D. degrees from the Massachusetts Institute of Technology (MIT), Cambridge, in 1991 and 1997, respectively.

In 1997, he joined the Laboratory for Electromagnetic and Electronic Systems, MIT, as a Postdoctoral Associate, and became a Research Scientist in the laboratory in 1999. In July 2001, he joined the Department of Electrical Engineering and Computer Science, MIT, where he is presently the Emanuel E. Landsman Associate Professor of Electrical Engineering and Computer Science. His research interests include design, manufacturing, and control techniques for power electronic systems and components, and in their use in a wide range of applications.

Dr. Perreault received the Richard M. Bass Outstanding Young Power Electronics Engineer Award from the IEEE Power Electronics Society, an ONR Young Investigator Award, the SAE Ralph R. Teetor Educational Award, and two IEEE Prize Paper Awards. He is a member of Tau Beta Pi and Sigma Xi.